Geophysica (2003), 39(1-2), 31-50

Modelling of Superimposed Ice Formation and Sub-Surface Melting in the Baltic Sea

Bin Cheng, Jouko Launianen and Timo Vihma

Finnish Institute of Marine Research
P.O. Box 33, FIN-00931 Helsinki, Finland

(Received: November 2002; Accepted: October 2003)

Abstract

Superimposed ice formation and sub-surface melting were modelled using a one-dimensional thermodynamic sea ice model with the Baltic Air-Sea-Ice Study (BASIS) field data. During a thermal equilibrium stage in winter 1997/98, ice showed little mass change at the ice-water interface. The observations indicated snow-to-ice transformation at the snow-ice interface. Numerical modelling suggested that the re-freezing of the surface melt water was the primary source of superimposed ice formation. A total of 5 of cm superimposed ice was modelled in BASIS-98. During early spring 1999, both observed and modelled ice temperatures indicated a sub-surface maximum at the melting point due to solar radiation penetrating below the surface. A 4.5 cm layer of snow melting was modelled, 20% of which was accounted for by sub-surface melting. The model results indicated that superimposed ice formation made a contribution to the total ice thickness during mid-winter, while sub-surface melting contributed to the total melting during early spring. Sensitivity studies indicated that total melting is sensitive to the snow's thermal properties, while sub-surface melting is sensitive to the snow's extinction coefficient.

Key words: Baltic Sea, sea ice thermodynamics, superimposed ice, sub-surface melting

1. Introduction

Various thermal and isostatic mechanisms in the snow layer have a strong impact on the thermodynamic modelling of sea ice. For instance, congelation ice growth at the ice bottom is much reduced by the presence of snow, since the thermal conductivity of snow is much smaller than that of ice. This large insulation effect of snow was the main issue considered in early sea ice thermodynamic models (e.g. *Maykut and Untersteiner*, 1971, *Semtner*, 1976, *Parkinson and Washington*, 1979). In recent decades, further attention has been paid to other aspects. In the presence of liquid water , the snow layer may contribute to the ice thickness via a snow-to-ice transformation. This may take place through various different physical processes. On the one hand, a heavy snow loading on top of the ice may cause a negative freeboard and subsequently sea-water flooding of the ice surface and basal snow. A salty slush layer may be generated that subsequently freezes above the original ice cover. On the other hand, melt water from

snow or rainfall may percolate downwards and refreeze above the original ice cover, to form a layer of fresh ice. The first process is called snow-ice formation due to ocean flooding (*Leppäranta*, 1983), while the second is called superimposed ice formation (*Kawamura et al*., 1997; *Haas et al*., 2001). Another striking process related to snow thermodynamics is internal melting. This is caused by the large amount of solar radiation penetrating into the snow in spring in sub-polar seas and also in summer in the Arctic and Antarctic (*Launiainen and Cheng*, 1998; *Liston et al.*, 1999).

The snow ice formation consequent on ocean flooding normally takes place in early winter in regions with a lot of snowfall, e.g. in the Baltic Sea and also in the Antarctic (*Leppäranta*, 1983; *Ackley et al*., 1990). Superimposed ice formation is well known in glacier research (*Paterson*, 1983). It is important for glacier mass balance, since it may act to temporarily buffer glaciers against rapid mass loss during climatic warming (*Pfeffer et al*., 1991). It has been also observed in both the Antarctic and Arctic sea ice fields (*Haas et al*., 2001). A recent expedition carried out in 2002 on first-year land-fast ice in Kongsfjorden, Svalbard, recorded that a total of 23 cm of snow was transformed into 5-6 cm of superimposed ice (*Haas et al*., 2002). Sub-surface melting is dominated by the effect the penetrating solar radiation. It is also sensitive to the thermal and optical properties of the snow/ice. This phenomenon has been reported as occurring in both the Arctic and Antarctic (*Schlatter*, 1972; *Brandt and Warren*, 1993; *Bøggild et al.*, 1995; *Koh and Jordan*, 1995; *Winther et al*., 1996; *Liston et al*., 1999).

The Baltic Sea is a seasonally ice-covered sea. The ice seasons last from a few weeks in the southern Baltic Sea to up to more than half a year in the far north. Early studies indicated that in the northern Baltic Sea from December to February, snowfall accounts on average for 25-45 mm equivalent water per month (*Kolkki*, 1969), and the snow ice may contribute to some 1/3 of the total ice thickness (*Leppäranta and Seinä*, 1982). Measurements made in the Gulf of Finland in winter 1998/99 indicated that as much as 43-55% of the total coastal land-fast ice was snow ice (*Kawamura et al*., 2001). The first attempt to model snow-ice formation via ocean flooding was made by *Leppäranta* (1983)**,** with attention being paid to the ice-growth season. The recent modelling study of *Saloranta* (2000) was focused on the seasonal variation in snow-ice formation in the Baltic Sea. The formation of superimposed ice was detected in a recent study by *Granskog et al*. (2003). Their studies of land fast ice properties during the winter seasons 1999-2001 indicated that the superimposed ice contributed up to 20% of total ice mass in a seasonal scale. The first-order modelling trials of sub-surface melting in the Baltic Sea has been made by *Launiainen and Cheng* (1998). Conclusive quantitative modelling of superimposed ice formation and sub-surface melting are**,** however, still lacking.

In this paper, we study superimposed ice formation and sub-surface melting using field data gathered from the Baltic Sea. Due to the limitation of in situ data, the ice model runs were made on a synoptic time scale. The primary motivation of this study is to quantitatively understand the effects of superimposed ice formation and sub-surface melting on sea ice thermodynamics. The ice model is described in section 2, while the

field expeditions and data are briefly introduced in section 3. The results and discussion are given in section 4, while the final conclusions are drawn in section 5.

2. Sea ice model

2.1 Basic model equations

The ice model presented by *Launiainen and Cheng* (1998) is used in this study. The model physics is basically the same as in *Maykut and Untersteiner* (1971), *Gabison* (1987), and *Ebert and Curry* (1993). Special attention is, however, paid to the parameterization of the air-ice fluxes and the solar radiation penetrating into the snow and ice. The heat conduction equation forms the central element of the ice model:

$$(\rho c)_{i,s}\frac{\partial T_{i,s}(z,t)}{\partial t}=\frac{\partial}{\partial z}\left(k_{i,s}\frac{\partial T_{i,s}(z,t)}{\partial z}\right)-\frac{\partial q_{i,s}(z,t)}{\partial z} \tag{1}$$

The subscripts *s* and *i* denote snow and ice, respectively. *T* is the temperature, *t* is time, and *z* is the vertical coordinate below the surface (positive downward). ρ is density, *c* is specific heat, and *k* is the thermal conductivity. The thermal conductivity and heat capacity of sea ice are given as: $k_i = k_{i0} + \beta s_i/(T_i - 273.15)$ and $(\rho c)_i = \rho_0 c_0 + \gamma s_i/(T_i - 273.15)^2$, following *Maykut and Untersteiner* (1971), where k_{i0}, ρ_0 and c_0 are the thermal conductivity, the density and the specific heat of pure ice, respectively, s_i is the ice salinity**,** and β and γ are constants.

The *q(z,t)* is the absorbed solar radiation, and is parameterized by a two-layer scheme adopted from *Grenfell and Maykut* (1977):

$$q_i(z,t)=i_0(1-\alpha_i)Q_s e^{-\kappa_i(z-\bar{z})}, \qquad z \geq \bar{z} \tag{2a}$$

$$q_i(z,t)=(1-\alpha_i)Q_s e^{-\kappa_{i0}z}, \qquad \kappa_{i0}=-10\times\ln(i_0) \quad 0<z<\bar{z} \tag{2b}$$

where α_i is the surface albedo of ice, Q_s is the incoming shortwave radiation at the surface and $(1-\alpha_i)Q_s$ is the net downward solar radiation at the surface (in the case of bare ice). The extinction coefficient κ_i is assumed to be 1.5 m^{-1} (*Untersteiner* 1961) and i_0 is defined as the fraction of the wavelength-integrated incident irradiance transmitted through the top $\bar{z}$ = 0.1 m of the ice. i_0 is the portion of solar radiation that does not directly contribute to temperature changes at the surface. It is parameterized as a function of sky conditions (cloud fraction, *C*) and sea ice colour. For example, $i_0 = 0.18(1-C) + 0.35C$ for white ice, and $i_0 = 0.43(1-C) + 0.63C$ for blue ice (*Ebert and Curry*, 1993; *Perovich* 1996). Within the top 0.1 m of the ice, we assume that radiation follows the exponential law and the extinction coefficient κ_{i0} is valid for the very uppermost layer**.** κ_{i0} is obtained by fitting the values of i_0 of *Grenfell and Maykut* (1977) observed at a depth of 0.1 m in the ice. For example, κ_{i0} = 17 m^{-1} for white ice and clear sky conditions. This assumption approximately satisfies the fact that κ_i can be one or two orders of magnitude larger than 1.5 m^{-1} near the surface, as found by *Grenfell and*

Maykut (1977). Such a two-layer scheme for $q_i(z,t)$ but with a linear profile fitted to the i_0 of *Grenfell and Maykut* (1977) has been used previously by *Sahlberg* (1988). In snow, the penetrating solar radiation is more consistent, following the Bouguer-Lambert law, i.e., $q_s(z,t) = (1-\alpha_s)Q_s e^{-\kappa_s z}$, where the extinction coefficient κ_s varies from 5 m^{-1} for dense snow up to almost 10 times larger for newly-fallen snow, depending on the snow density and grain size (*Perovich,* 1996).

The surface heat balance reads:

$$(1-\alpha_{i,s})Q_s - I_0 + \varepsilon Q_d - Q_b(T_{sfc}) + Q_h(T_{sfc}) + Q_{le}(T_{sfc}) + F_c(T_{sfc}) - F_m = \Gamma(T_{sfc}) = 0 \qquad (3)$$

where the subscript *sfc* refers to the surface (can be either snow or bare ice). The downward short-wave radiation (Q_s) is calculated by an empirical formula (*Shine*, 1984) with the cloudiness factor of *Bennett* (1982):

$$Q_s = \frac{S_0 \cos^2 Z}{\left[(\cos Z + 1.0)\cdot e \cdot 10^{-3} + 1.2\cos Z + 0.0455\right]}(1 - 0.52C) \qquad (4)$$

where S_0 is the solar constant, Z is the local solar zenith angle, e is the vapour pressure (in hPa) and C is from 0 to 1.

The incoming atmospheric long-wave radiation (Q_d) is calculated by the formula of *Efimova* (1961) with the cloud effect according to *Jacobs* (1978):

$$Q_d = (0.746 + 0.0066\cdot e)\cdot \sigma_a \cdot T_a^4 \cdot (1 + 0.26C) \qquad (5)$$

where σ is the Stefan-Boltzmann constant and T_a is the air temperature. The outgoing longwave radiation from the surface is estimated by the Stefan-Boltzmann law $Q_b = \varepsilon\sigma T_{sfc}^4$ with a constant surface emissivity ($\varepsilon = 0.97$). Finally, the net longwave radiation used for the surface heat balance is $\varepsilon Q_d - Q_b$.

The fluxes of turbulent sensible heat (Q_h) and latent heat (Q_{le}) are calculated by the bulk formulae:

$$Q_h = -\rho_a c_p C_H (\Theta_{sfc} - \Theta_{za}) V_{za} \qquad (6)$$

$$Q_{le} = -\rho_a L_v C_E (q_{sfc} - q_{za}) V_{za} \qquad (7)$$

where ρ_a is the air density, c_p is the specific heat of air, L_v is the enthalpy of vaporization, C_H and C_E are the turbulent transfer coefficients, Θ the potential temperature, V the wind speed, and q the specific humidity. The subscript *za* refers to a height of *za* in the air. The coefficients C_H and C_E are estimated using the Monin-Obukhov similarity theory with stability effects based on *Högström* (1988) in unstable cases and *Holtslag and de Bruin* (1988) in stable cases. A value of 0.001 m is used for the aerodynamic roughness length, and the thermal roughness length is calculated according to *Andreas* (1987).

The surface conductive heat flux is F_c, and the heat consumed in surface melting is F_m. When T_{sfc} would to be higher than the freezing temperature (T_f), T_{sfc} is constrained to remain at T_f, and the excess heat is used for melting. $F_m = \rho_{i,s} \cdot L_f \cdot dh_{i,s}/dt$, where L_f is the latent heat of fusion, assumed to be constant, and $h_{i,s}$ is the thickness of ice or snow. The heat balance equation (3) can also be seen as a polynomial in the surface temperature $\Gamma(T_{sfc})$ once the external forcing is specified. The temperature T_{sfc} is calculated iteratively from (3) and is used as the upper boundary condition for the numerical scheme of (1).

In the case of a snow cover on top of the ice, equation (1) is applied for both the snow and the ice layers. The ice-snow interface temperature is calculated via a flux continuity equation:

$$k_s \, \partial T_s / \partial z \big|_{snow} = k_i \, \partial T_i / \partial z \big|_{ice} \tag{8}$$

At the ice bottom:

$$T_{bot} = T_f \tag{9a}$$

$$-\rho_i L_f \, dh_i/dt = -(k_i \, \partial T_i / \partial z)_{bot} + F_w \tag{9b}$$

where the ice bottom temperature (T_{bot}) is constrained to be at the freezing temperature and F_w is the oceanic heat flux, assumed constant. The model parameters are listed in Table 1, and are based on values given in the literature and on field measurements in the Baltic Sea.

Table 1. Model parameters based on BASIS measurements and the literature.

Symbol	Name	Value	Note
Z_o	Aerodynamic roughness	10^{-4} m	Launiainen and others (2001)
κ_I	Extinction coefficient of sea ice	1.5 - 17 m^{-1}	Modified from Maykut & Grenfell (1977)
κ_s	Extinction coefficient of snow	15 - 25 m^{-1}	Perovich (1996)
T_f	Freezing point	-0.2 – 0.26 °C	$Tf \approx -0.054 \cdot s_w$
$(\rho \cdot c)_i$	Sea ice volumetric heat capacity	function of T_i, and s_i	Maykut and Untersteiner (1971)
c_p	Heat capacity of ice	2093 J kg^{-1} K^{-1}	
L_i	Latent heat of freezing	0.33×10^6 J kg^{-1}	
F_w	Oceanic heat flux	1.0 W m^{-2}	Eddy-flux measurements in BASIS-98
ρ_i	Sea ice density	910 kg m^{-3}	
s_i	Sea ice salinity	0.38 – 0.75 ppm	Ice core measurement in BASIS-(98,99)
s_w	Sea water salinity	3.7 – 4.9 ppm	Measurements in BASIS-(98,99)
ρ_s	Snow density	150 - 380 kg m^{-3}	Measurements in BASIS-(98,99)
ε	Surface emissivity	0.97	Assumed
k_{si}	Sea ice heat conductivity	function of T_i, and s_i	Maykut and Untersteiner (1971)
k_i	Thermal conductivity of ice	2.03 W m^{-1} K^{-1}	
k_s	Thermal conductivity of snow	0.056 - 0.24 Wm^{-1} K^{-1}	Calculated according to Yen (1981), and Sturm (1997).

The ice model equations (1)-(9) are solved by a conservative difference numerical scheme (*Cheng*, 1996). This scheme is essentially similar to that of Crank-Nicholson, but applies a more flexible tuning from explicit to implicit using a single parameter. It is derived by the integral interpolation method, a numerical technique that ensures that the scheme is easily extended to an uneven spatial resolution (*Cheng*, 2002).

2.2 Calculation of superimposed ice formation and sub-surface melting

According to its definition, the formation of superimposed ice refers to a snow-to-ice transformation. This process is assumed to occur at the snow-ice interface. The surface melting of snow or rainfall yields the water supply for re-freezing. The downward percolation of water may take time, depending on the snow thickness. For the sake of simplicity, we assume that the supplied water is at the freezing point and percolates down to the snow-ice interface without delay. In particular, the time lag of heat conduction within the ice due to the percolation of water to the snow-ice interface is assumed to be zero. This is justified, because the modelling periods of our study are 18 and 7 days, during which the major changes in the snow and ice temperature take place on time scales of a few hours to a few days, while the time scale of melt water percolation is of the order of minutes to tens of minutes. A simple mass balance equation is applied to the water-saturated snow layer before it totally re-freezes to superimposed ice (H_i). Accordingly, we have the equation of time change of enthalpy as:

$$-\rho_i L_f \, dH_i \,/dt = (k_s \, \partial T_s / \partial z)\big|_{z=h_s} - (k_i \, \partial T_i / \partial z)\big|_{z=h_i} \tag{10}$$

Once we apply this equation, the snow-ice interface temperature will be naturally restored to the freezing point. Equation (10) is actually calculated for freezing at the snow-ice interface. Under mild weather condition, instead of freezing, a slush layer may remain at the snow-ice interface. Melting and rainfall are taken into account as equivalent water, and (10) is confined to the re-freezing of the total available equivalent water. This procedure approximately satisfies the need for energy conservation. One shortcoming is that the re-freezing may in reality create a thicker superimposed ice layer than that based on the thickness of the superimposed water layer only. This is because when the water supply reaches the snow-ice interface, it normally fills the pores in the snow, and this mixture of water and snow naturally takes up more space than water alone would take. On the other hand, the snow becomes more compact due to the presence of water.

Equation (10) describes macroscopic processes, which means that the re-freezing and melting depend merely on the heat flux divergence. The processes occurring on a real microscopic scale, such as the draining of melt water and the evolution of snow density and grain structure, were not taken into account. For details of these complex processes involved in snow melting and re-freezing, see the pioneering work by *Pfeffer et al.* (1990), and *Pfeffer and Humphrey* (1996, 1998).

Sub-surface melting may occur due to the shortwave radiation absorbed in the snow and ice. The calculations are based on the equations of conductive heat flux and absorbed solar radiation in various snow/ice layers. For a sub-surface layer with its calculated temperature higher than the melting point, the temperature will remain at the melting point, and the excess heat will be used for melting, and a thinner snow layer will be obtained. Figure 1 schematically indicates the sub-surface melting. For a single inner grid level at the melting point, a sub-layer is considered to be half a grid distance from this point both upwards and downwards (Fig. 1a). Figure 1b shows the case with 2 grid levels at the melting point.

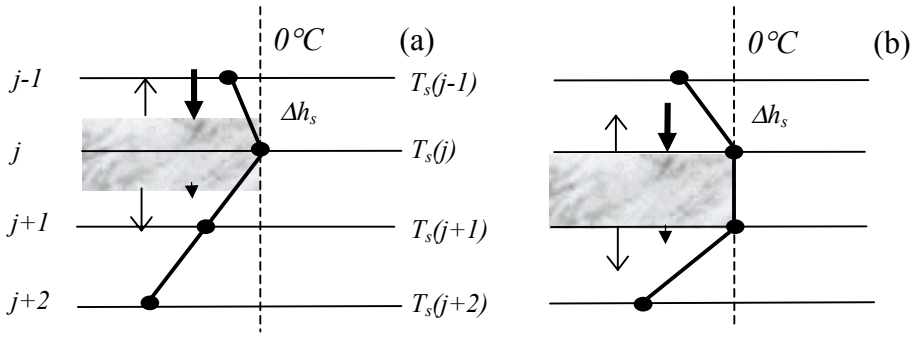

Fig. 1. Model grid system for the calculation of sub-surface melting. The model grids levels are marked by horizontal lines and the temperature profile by a thicker line connecting the dots. The thin arrows indicate the conductive heat flux between a sub-surface layer and adjoining layers. The thick arrows indicate the solar radiation penetrating through the sub-surface layer. Δh_s is the model grid size in snow. $T_s(j)$ is the snow temperature at grid level j.

For cases (a) and (b) in Figure 1, the respective calculations are made using:

$$\rho_s L_f \, dh_s/dt = -\left[(k_s \, \partial T_s/\partial z)\Big|_{j\Delta h_s/2} + (k_s \, \partial T_s/\partial z)\Big|_{(j+1)\Delta h_s/2}\right] + (1-\alpha_s) Q_s (e^{-k_s(j)\Delta h_s/2} - e^{-k_s(j+1)\Delta h_s/2}) \tag{11a}$$

$$\rho_s L_f \, dh_s/dt = -\left[(k_s \, \partial T_s/\partial z)\Big|_{j\Delta h_s} + (k_s \, \partial T_s/\partial z)\Big|_{(j+1)\Delta h_s}\right] + (1-\alpha_s) Q_s (e^{-k_s(j\Delta h_s)} - e^{-k_s(j+1)\Delta h_s}) \tag{11b}$$

For sub-surface melting within the sea ice, the principle of calculation is the same, but the penetrating solar radiation is considered in a more complicated way according to (2a, 2b). Again, we have also made some assumptions, for simplicity. For example, if sub-surface melting occurs in the ice layer, the melt water is simply removed from the total ice layer, which accordingly becomes thinner. If it occurs in the snow layer, the layer also becomes thinner, but the melt water is considered as a part of the water supply and will be present at the snow-ice interface, and may refreeze there. The change in the thermal conductivity of snow and ice due to sub-surface melting is not taken into account.

3. Forcing data

Data from two winter expeditions were applied in this study. The data were obtained from BASIS, which was a project of the GEWEX-BALTEX program. The main field campaign, BASIS-98, was organised in winter 1997/98 in the Gulf of Bothnia, in the northern Baltic Sea. In the following winter, a less extensive ice expedition BASIS-99 was carried out. The locations of the two field experiments were 125 km from each other, both some 3 km from the coast in the land-fast ice region. During BASIS-98, the surface conditions were variable. Snowfall was occasionally observed, and drifting snow occurred frequently due to strong winds. In contrast, the ice bottom showed little change, indicating a stage of thermal equilibrium. Observations indicated snow-to-ice transformation at the snow-ice interface. The ice thermistor string was deployed through the snow and ice layers just before a cold-air outbreak started, and the string was successfully refrozen with surrounding water. Details of the measurements, methods and instrumental arrangements in BASIS-98 can be found in *Vihma et al*. (1999), and *Shirasawa and Kobinata* (1999).

During the BASIS-99 field experiment, the average snow thickness on the ice was approximately 20 cm, and snow drifting was weak. Some 9 cm of new snow accumulated during our measurements, and surface melting was seen. The average total ice thickness was 45 cm. The ice thermistor string was deployed during cold weather, as in BASIS-98, to be sure that the sensors froze in the snow and ice, However, to prevent artificial flooding, the whole ice layer was not penetrated by the thermistor stick. To prevent absorption of solar radiation by the stick, a wooden plate was installed on the snow 1 m south of the stick. Table 2 gives basic information on these two expeditions.

Table 2. The basic weather and ice information during the field experiments.

Time	BASIS-98 (18 days)	BASIS-99 (7 days)
	16 Feb. – 7 March	19 - 26 March
Location	63°08.12'N, 21°14.67'E	63°55.05'N, 22°56.72'E
Weather conditions (average):		
wind speed V_a(10m)	7.6 ms^{-1}	4.7 ms^{-1}
air temperature T_a (10m);	-4.3 °C	-1.6 °C
relative humidity Rh (4.5m)	78 %	84 %
T_a > 0.0 °C (portion of data)	39 %	20 %
downward solar radiation Q_s (daytime average)	139 Wm^{-2}	188 Wm^{-2}
mean surface albedo (α_s)	0.73	0.81
Average ice thickness	38.6 cm	44.6 cm
Snow properties:		
soft snow	3 cm (at the beginning)	9 cm (new snow)
hard snow	3.5 cm (at the beginning)	18 cm (old snow)
average snow thickness	4.3 cm	23.1 cm
Ice freeboard	1.4 cm	-7.9 cm

The basic meteorological measurements to support the ice modelling study were made using a weather mast (wind, temperature and relative humidity), a sonic anemometer (turbulent heat and momentum fluxes), pyranometers, infrared thermometers, and net-radiometers (radiative fluxes), an ice thermistor string (ice and snow temperatures), and an ultrasonic current meter (heat flux from the ocean below the ice). Ice core samples were collected for ice salinity. The ice and snow thickness and freeboard were manually measured every day. The weather data, solar radiation and surface albedo were used as the external forcing for the model.

4. Results and discussion

The weather in BASIS-98 and BASIS-99 were clearly quite different. Figure 2 shows the time series of air temperature and the melting periods in both BASIS-98 and BASIS-99. In BASIS-98, the melting periods occurred between much colder periods. This suggests that superimposed ice formation may have occurred. In BASIS-99, the air

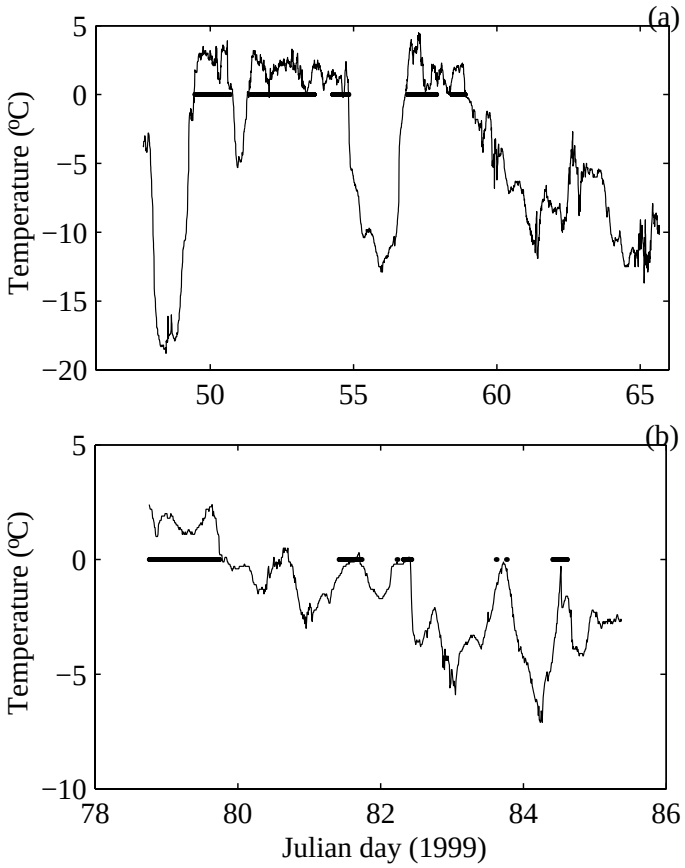

Fig. 2. The air temperature time series during (a) BASIS-98 and (b) BASIS-99. The horizontal lines indicate the melting periods.

temperature was less cold, and several melting periods were detected. The air temperature seems to be a response to the diurnal cycle of solar radiation. The conditions favoured sub-surface melting, because the expedition was carried out in the

early spring when there was substantial solar radiation. The following discussion accordingly focuses on superimposed ice formation in BASIS-98 and sub-surface melting in BASIS-99.

4.1 Superimposed ice formation in BASIS-98

General ice modelling with BASIS-98 data was described in *Cheng et al*. (2001), but without quantitative attention to the superimposed ice formation. During the expedition, there were three periods with the air temperature well above zero, during which five separate melting periods can be seen (Fig. 2a; note that a 2-m air temperature above zero does not necessarily indicate melting). During the melting periods, the downward net heat flux into the snow layer was modelled. During the cold period on Julian days 55 to 57, very strong upward heat flux can be seen in both the snow and the ice (Fig. 3). The modelled surface melting during the whole study period was about 12 cm in snow thickness. The modelled re-freezing of melted snow to superimposed ice and the cumulative total ice thickness compared with the average observed ice thickness are shown in Figure 4. The total superimposed ice formation was about 5 cm (Fig. 4b). The calculation indicated that the re-freezing of previously-melted snow was completed within the time-scale of the cold periods (Figs. 2 and 4b). The total re-freezing was limited by the surface water supply, which in this case was mainly due to the surface melting of snow.

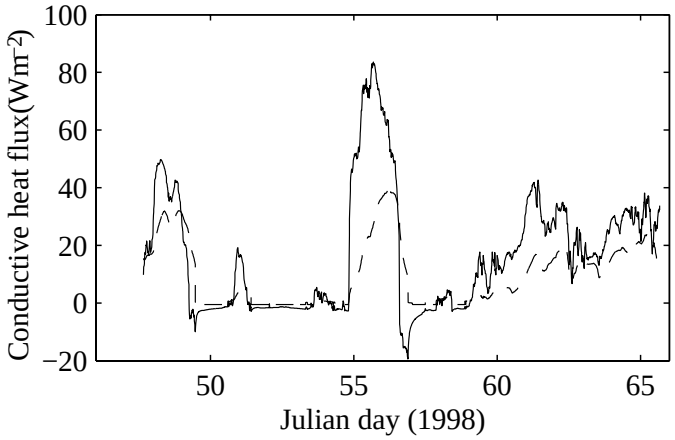

Fig. 3. The modelled average conductive heat flux in snow (solid line) and ice (dashed line) during BASIS-98.

The total ice growth was mainly due to the superimposed ice formation (Fig. 4c). Figure 5 shows the measured snow and ice thickness and the water level with respect to the snow-ice interface, as well as the in-ice temperatures. The freeboard along a 50-m long L-shaped observation line in the vicinity of the thermistor string was occasionally negative. On a couple of days, the snow-ice interface temperature reached the freezing point. The observations also indicate snow to ice transformation. At the beginning, when we deployed the ice thermistor string, the ice thickness was 34 cm. The snow depth was 6.5 cm, of which 3 cm was soft snow and 3.5 cm was hard snow. The up-

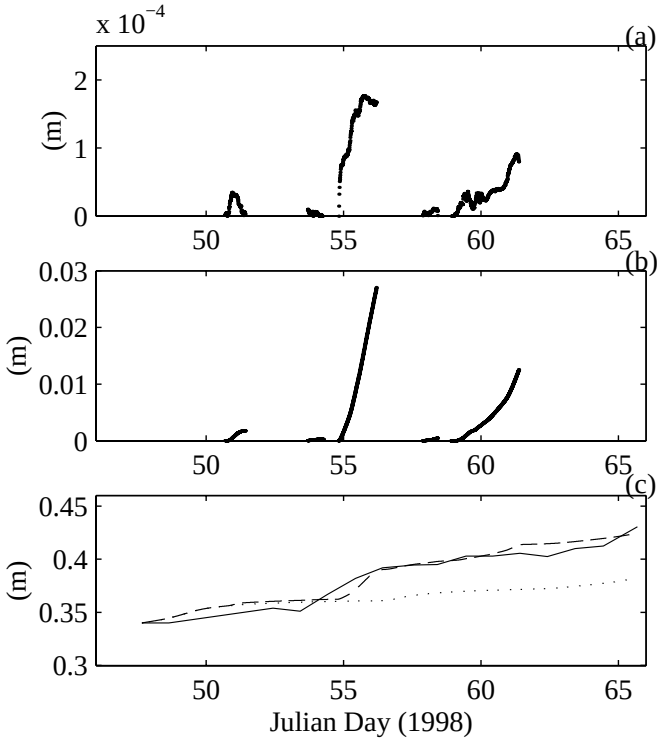

Fig. 4. The superimposed ice formation and cumulative ice thickness in BASIS-98. (a) Re-freezing of surface melt water during each 10-minute time-step; (b) accumulated superimposed ice thickness during each re-freezing period; (c) the modelled cumulative total ice thickness (dashed line) compared with the observed average ice thickness (solid line) and the ice growth at the ice bottom (dotted line).

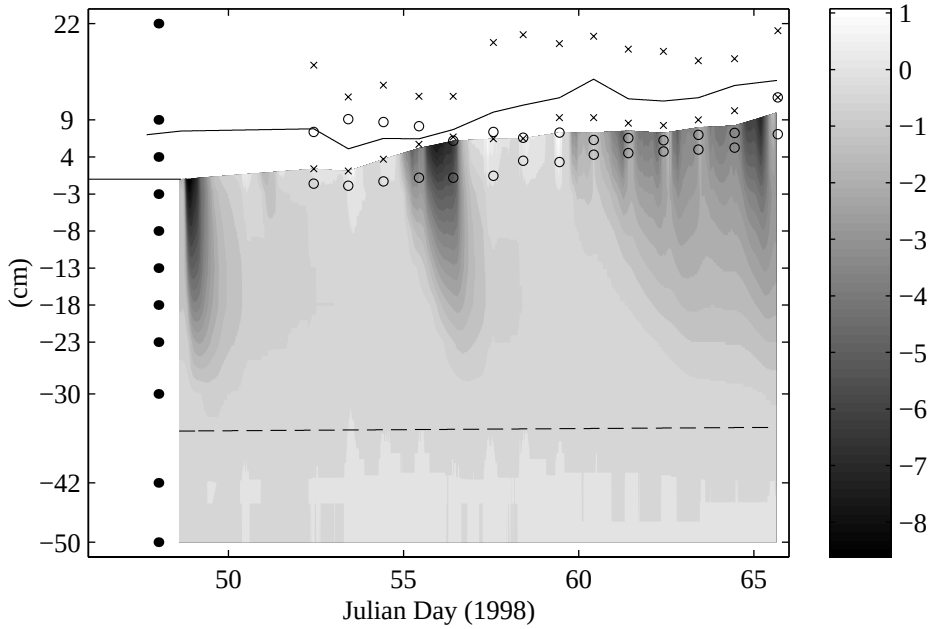

Fig. 5. Snow, ice thickness, water level (relative to the snow/ice interface) and ice/water temperature field measurements in BASIS-98. The filled circles indicate the locations (relative to the snow-ice interface) of the sensors of the thermistor string (sensor 1 at the lowest and sensor 11 at the highest level) deployed in the ice field. The time series of symbols (×) and (o) give the maximum and minimum snow thicknesses and water level, respectively, observed along a 50-m long line. The solid line at the top is the average snow thickness. The lowest dashed line is the ice bottom detected from the thermistor string between the initial deployment and final pick-up stage.

permost of the ten temperature sensors (sensor 10) was 1.5 cm above the snow surface (Fig. 5). Seven sensors were inside the snow or ice, the lowest of them (sensor 3) 5 cm above the ice bottom. Sensors 1 and 2 were in the water. The depths of the sensors relative to the snow and ice changed in time, as shown in Figure 5. At the end of BASIS-98, the total ice thickness was 40 cm. Light snowfall occurred during the expedition. We conclude that the snow-to-ice transformation was mainly due to the formation of superimposed ice and this was also borne out by the observations.

4.2 Sub-surface melting in BASIS-99

During BASIS-99, both snowfall and surface melting were seen, and 20% of the data indicated an air temperature well above the freezing point. The daytime average solar radiation was 35% larger than in BASIS-98.

The snow was essentially divided into two layers, representing soft new snow on top of a wind-slab of hard old snow. The average snow densities were 150 and 380 kg m^{-3}, respectively (M. Lundin, Swedish Meteorological Hydrological Institute, personal communication). According to *Sturm* (1997), these correspond to thermal conductivities of 0.056 and 0.23 $Wm^{-1}K^{-1}$, respectively. Following *Perovich* (1996), we further estimated the snow extinction coefficients as 25 and 15 m^{-1} for the upper and lower layers, respectively. The modelled snow melting is shown in Figure 6. The total melting was about 4.5 cm, of which about 20% is accounted for by sub-surface melting. The evolution of the snow thickness is given in Figure 7. The snow accumulation was larger than in BASIS-98, but surface melting was also critical in controlling the snow evaluation.

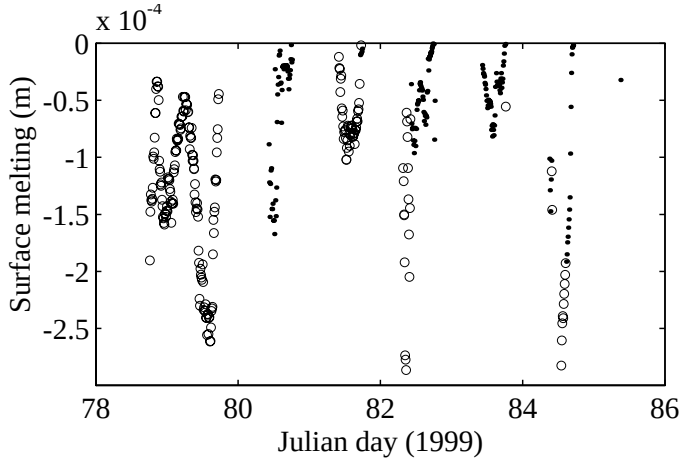

Fig. 6. Modelled snow melting in BASIS-99. The circles are the surface melting while dots are the calculated sub-surface melting. The melting value corresponds to a time-step of 10 minutes.

The observed and modelled snow and ice temperature fields are shown in Figure 8. Unfortunately, the uppermost thermistor recorded unreliably high snow temperatures and thus is not shown here. Radiative heating of the uppermost sensors in snow or ice can lead to incorrect temperature measurement (*Brandt and Warren*, 1993).

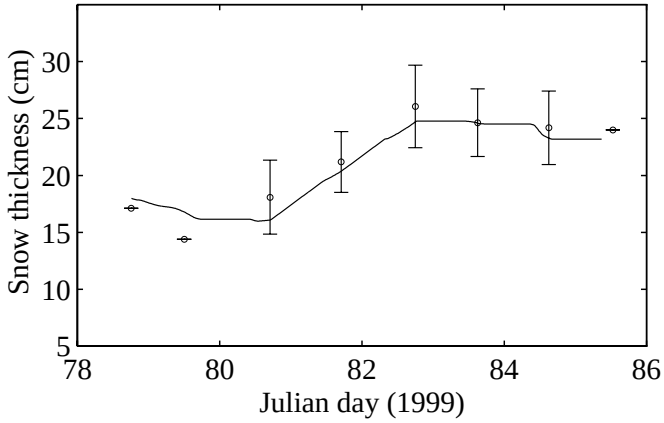

Fig. 7. The time-series of snow thickness in BASIS-99. The dots give the observed daily mean together with ± standard deviation (vertical bars). The solid line shows the modelled result.

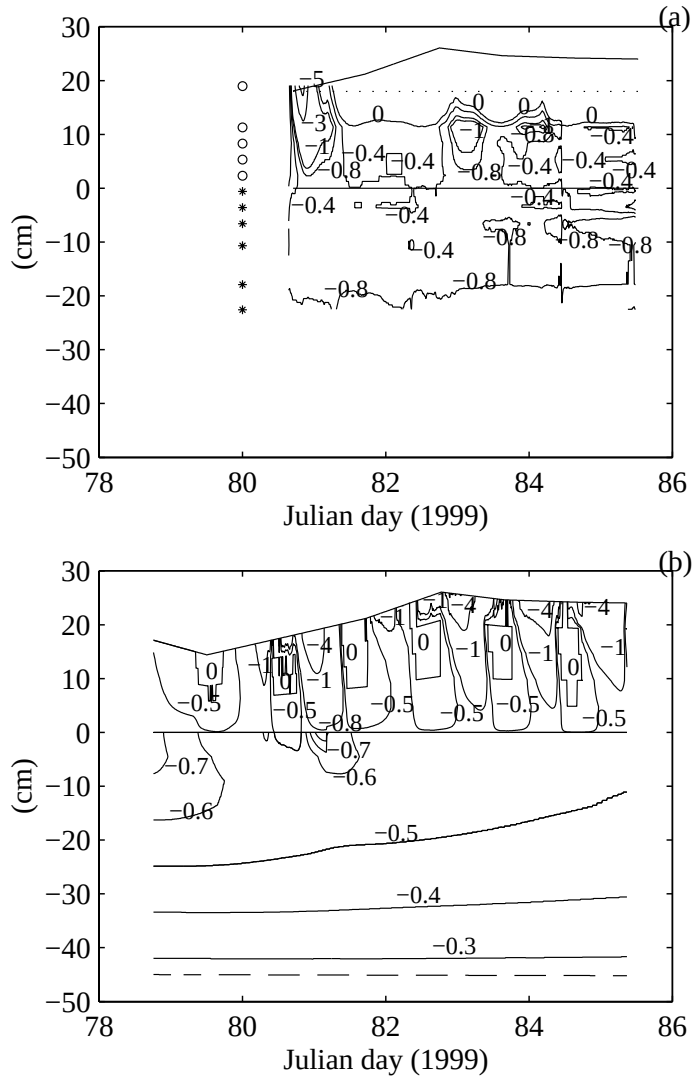

Fig. 8. Snow and ice temperature (°C) during BASIS-99 experiment, (a) observed by the thermistor string, and (b) modelled. The symbols o and ∗ in (a) show the locations of the temperature sensors in the snow and ice, respectively. The dashed line in (b) indicates the ice bottom.

Both measurements and calculations indicated sub-surface temperatures of up to 0°C. The results showed that the sub-surface melting was located within a layer centered about 10 cm below the surface. The model results show a diurnal variation in snow temperature, while the measurements suggest the same only for the first day after deployment of the thermistor stick. From the second day of the expedition onwards, the observed snow/ice temperature regime was rather isothermal. On the one hand, this is probably due to the effect of the wetness of the snow layer, since the snowfall was occasionally mixed with rain. The latent heat of the water fraction in snow can damp the daily temperature variation in the snow layer. On the other hand, the snow thickness was much above the threshold for ocean flooding. Although the deployment of the thermistor stick was very careful, to avoid penetrating the whole ice layer, ocean water may still have seeped up to the snow-ice interface. The effect of snow wetness was not taken into account in the model. Further studies of this aspect are needed.

Some sensitivity tests were carried out in order to see the effect of various snow properties on the melting. For simplicity, the snow is assumed to be a homogeneous layer in each model run. A total of 100 model runs were carried out with different combinations of snow density, thermal conductivity, and extinction coefficient. The snow density was varied from 100 to 550 kg m^{-3}, while the thermal conductivity was calculated according to *Sturm et al*. (1997): $k_s = 10^{(0.002650\rho_s - 1.652)}$, $\rho_s \leq 600$. The extinction coefficient was varied from 5 to 50 m^{-1}. The forcing data were all from BASIS-99. The modelled total melting and sub-surface melting are shown in Figure 9. It can be seen that the total melting is more sensitive to the snow's thermal properties, while the sub-surface melting is sensitive to the snow's extinction coefficient. Such conclusions support the earlier studies of increased sub-surface temperature and sub-surface melting made by *Koh and Jordan* (1995), who employed high-resolution frequency-modulated continuous wave radar to detect the onset of sub-surface melting. Our sensitivity tests were confined to the current model assumptions, i.e., the heat conductivity depended on the snow density, while the extinction coefficient was independent of both these properties. In reality, interaction among all the parameters is to be expected, and this can affect both melt-layer thickness and sub-surface temperatures (*Bøggild et al*. 1995). Modelling of increased sub-surface temperature and sub-surface melting by taking into account such complex interactions among all the parameters has not been carried out so far.

4.3 Discussion

During BASIS-98, the downward solar radiation was small, and the surface melting was 12 cm in snow thickness. Taking into account the sub-surface melting, only 0.5 cm more melting was modelled. During BASIS-99, the downward solar radiation was 35% larger, and the sub-surface melting was substantial. The modelled conductive heat flux in snow and ice suggested, however, an almost isothermal stage (cf. Figure 8), and a calculation based on (10) produced practically no re-freezing, Neither was it indicated by the *in situ* observations.

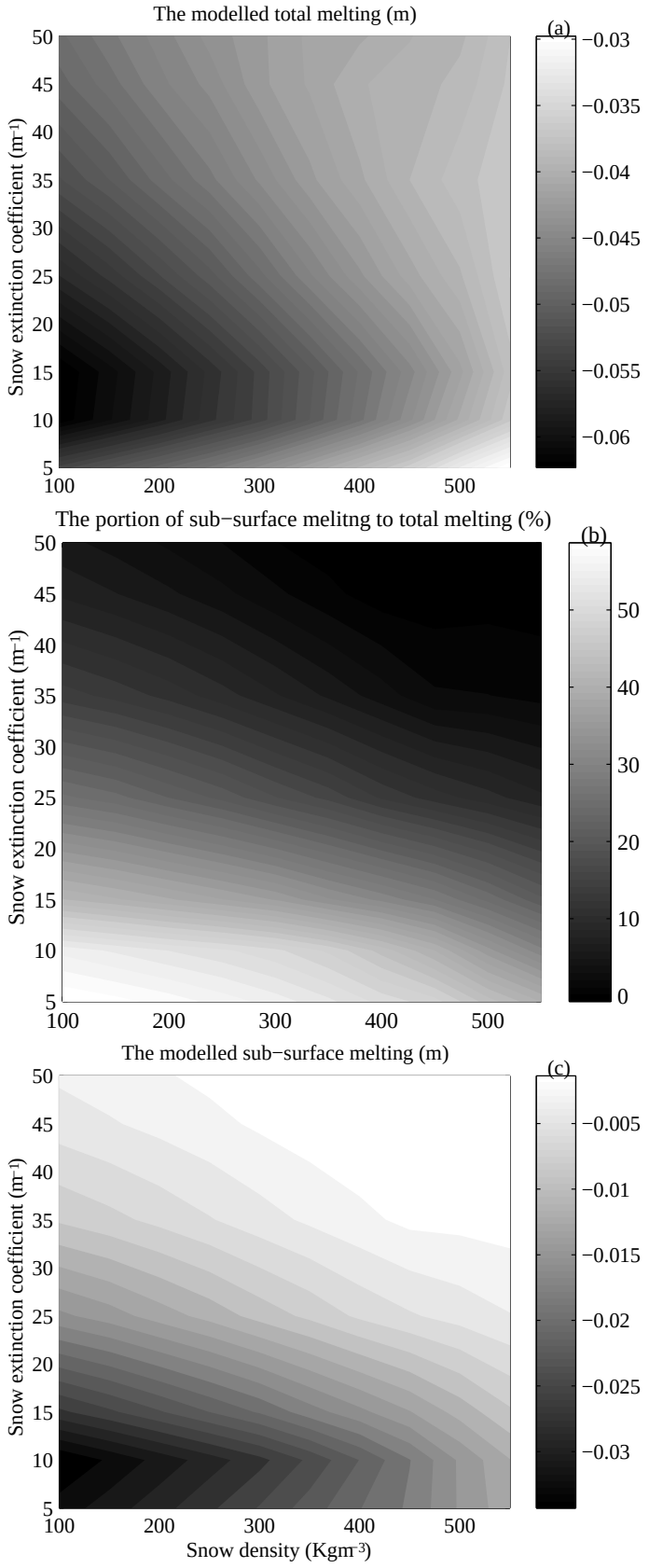

Fig. 9. Model sensitivity studies of the total melting and sub-surface melting as a function of the snow properties, (a) the total melting, (b) the percentage of sub-surface melting of the total melting, and (c) the sub-surface melting.

Ocean flooding is an important source for the formation of a slush layer and snow-ice (e.g. *Leppäranta*, 1983, *Saloranta*, 2000). It depends on the thickness of snow h_s and ice h_i, as well as on the densities of sea water (ρ_w), sea ice (ρ_i) and snow (ρ_s). Assuming that $\rho_i \approx 0.9\ \rho_w$ (The Baltic Sea is almost a fresh water body with a low surface salinity), according to Archimedes' law, the criterion for ocean flooding is (a) $h_s \geq 0.6\ h_i$ for very light snow, i.e. $\rho_s = 0.15\ \rho_{sw}$, and (b) $h_s \geq 0.2\ h_i$ for very dense snow, i.e. $\rho_s = 0.5\ \rho_{sw}$.

In BASIS-98, the snow density was about $0.3\ \rho_{sw}$ (*Lundin et al*., 1999), and h_s should accordingly be larger than approximately $0.3\ h_i$ for ocean flooding to occur. The measurements showed only a few occasions on which the maximum water level was above the ice surface (i.e., the freeboard was negative) and the snow thickness simultaneously matched the criterion of $h_s > 0.3\ h_i$. For most of the data with negative freeboard, the snow thickness did not even match (b). We believe that in these cases the reason for the negative freeboard was the percolation of surface melt water rather than ocean flooding. The snow-to-ice transformation due to the ocean flooding of land-fast ice depends on snow and ice thicknesses on a scale of at least tens of metres (*Lundin and Omstedt*, 2001). Moreover, we emphasise that the above-mentioned criterion for flooding is largely based on the assumption that water paths should be freely available. For land-fast ice, however, such a condition is not always satisfied, and the modelling of a slush layer based on Archimedes' law may lead to an overestimation of the formation of snow-ice (e.g. *Eicken et al*., 1995; *Saloranta*, 2000). By contrast, during BASIS-99 the ocean flooding criterion was well matched with the snow and ice thickness measurements: the average freeboard was -7.9 cm.

5. Conclusion

We summarize our interpretation of the observations and model results as follows. In BASIS-98, surface melting was substantial due to periods of above-zero air temperature, but sub-surface melting was minor due to insufficient solar radiation. It only added 4% to the surface melting. Surface melt water that had percolated to the snow-ice interface was responsible for the cases of negative freeboard. During the cold-air outbreaks, superimposed ice formation occurred via refreezing of the surface melt water. The snow cover was not thick enough to cause snow-ice formation via ocean flooding. In BASIS-99, the observed daytime average solar radiation in March was 35% larger than that in BASIS-98. Hence, it was strong enough for subsurface melting, contributing 20% of the total melting. The snow cover was thick enough for ocean flooding. The weather was, however, so mild that practically no refreezing took place during the period. It remains unclear whether significant refreezing occurred after the study period, or whether most of the melt water remained liquid in the snow pores and as a slush layer above the original ice.

The model results indicated that superimposed ice formation made a contribution to the total ice thickness during a thermal equilibrium period, while sub-surface melting made a contribution to the total melting during early spring. Further sensitivity studies

indicated that total melting is sensitive to the thermal properties of the snow, while sub-surface melting is sensitive to the extinction coefficient of the snow.

In this study, the water supply for superimposed ice formation was derived mainly from melting. In the Baltic Sea climate, wet snowfall and rainfall may occur in warm periods during the ice season, increasing the supply of liquid water. In general, although not observed in BASIS-98, ocean flooding is also supposed to be an important source for snow-to-ice transformation. Hence, accurate data on precipitation and its phase are important for the modelling of the snow-to-ice transformation on a seasonal scale.

We modelled the sub-surface melting quantitatively, but the model results were difficult to verify experimentally due to the problems encountered in measuring the temperature profile using temperature sensors embedded in the snow and ice. To verify such modelling results, more work is needed both on theoretical considerations and on field observations. We have to emphasize that the calculations made in this paper are restricted by the simplifications in the model parameters. For example, the effect of melt-water in the snow and ice is not taken into account when specifying values for the extinction coefficient, heat conductivity and density. This is because experimental results on this aspect are lacking. For this reason, too, new field experiments are needed.

Due to their important role in ice mass balance, superimposed ice formation and sub-surface melting are probably even more important for glaciers. The effect of these processes in sea ice thermodynamics should not, however, be ignored. In general, current thermodynamic sea ice models do not take the re-freezing of melted snow into account in the total mass balance. It should be included in future modelling studies with dynamic-thermodynamic sea-ice models.

Acknowledgement

We are grateful to the participants in the BASIS field experiments, in particular to Pekka Kosloff, Tero Purokoski, Henry Söderman and Hannu Vuori for field assistance and to Kunio Shirasawa for providing us with his under-ice heat flux data. We thank two anonymous reviewers for their constructive comments and insightful reviews of this paper. The study is part of the EC-supported BALTEX-BASIS project under contract MAST3-CT97-0117.

References

Ackley, S.F., M.A. Lange and P. Wadhams, 1990. Snow cover effects on Antarctic sea ice thickness. In: Ackley, S.F. and W.F. Weeks(eds.), Sea ice properties and processes, *US Army Cold Region Research and Engineering Laboratory*, *Monograph* **90-1** Hanover NH, USA, 16-22.

Andreas, E.L., 1987. A theory for the scalar roughness and the scalar transfer coefficients over snow and sea ice, *Boundary-Layer Meteorol.,* **38**, 159-184.

Bennett, T.J., 1982. A coupled atmosphere-sea ice model study of the role of sea ice in climatic predictability, *J. Atmos. Sci.,* **39**, 1456-1465.

Brandt, R.E. and S.G. Warren, 1993. Solar-heating rates and temperature profiles in Antarctic snow and ice, *J. Glaciol*., **39 (131)**, 99-110.

Bøggild, C.E., J.G . Winther, K. Sand and H. Elvehoy, 1995. Sub-surface melting in blue-ice fields in Dronning Maud Land, Antarctica: Observation and modelling, *Ann. Glaciol*., **21**, 162-68.

Cheng, B., 1996. The conservative difference scheme and numerical simulation of a one-dimensional thermodynamic sea ice model, *Marine Science Bulletin* (Chinese Journal), **15 (4)**, 8-15. (English translation in Finnish Institute of Marine Research -Contributions. No. 5).

Cheng, B., J. Launiainen, T. Vihma and J. Uotila, 2001. Modelling sea ice thermodynamics in BALTEX-BASIS, *Ann. of glaciology*, **33**, 243-247.

Cheng, B., 2002. On the modelling of sea ice thermodynamics and air-ice coupling in the Bohai Sea and the Baltic Sea, *Finnish Institute of Marine Research – Contributions* No. **5**, 38 pp. (Ph.D thesis)

Ebert, E.E. and J.A. Curry, 1993. An intermediate one-dimensional thermodynamic sea ice model for investigating ice-atmosphere interaction, *J. Geophys. Res.*, **98 (C6)**, 10,085-10,109.

Efimova, N.A., 1961. On methods of calculating monthly values of net long-wave radiation. *Meteorol. Gidrol.*, **10**, 28-33.

Gabison, R., 1987. A thermodynamic model of the formation growth and decay of first-year sea ice, *J. Glaciol.*, **33(113)**, 105-109.

Granskog, M.A., M. Leppäranta, T. Kawamura, J. Ehn and K. Shirasawa, 2003. Seasonal development of the properties and composition of landfast sea ice in the Gulf of Finland, the Baltic Sea, *J. Geophys. Res.,* in press.

Haas, C., D.N. Thomas and J. Bareiss, 2001. Surface properties and processes of perennial Antarctic sea ice in summer, *J. Glaciol*., **47 (159)**, 613-625.

Haas, C., J. Bareiss and M. Nicolaus, 2002. The surface energy balance and its importance for superimposed ice formation, A report for the LSF project NP-9/2001: SUBISUP 2002. Online publication at: http://www.awi-bremerhaven.de/ modelling/seaice/

Holtslag, A.A.M. and H.A.R. de Bruin, 1988. Applied modelling of the nighttime surface energy balance over land, *J. Appl. Meteorol.,* **37**, 689-704.

Högström, U., 1988. Non-dimensional wind and temperature profiles in the atmospheric surface layer: A re-evaluation, *Boundary-Layer Meteorol.,* **42**, 55-78.

Kawamura, T., K.I. Ohshima, T. Takazawa, and S. Ushio, 1997. Physical, structural and isotopic characteristics and growth processes of fast sea ice in Lützow-Holm Bay, Antarctica, *J. Geophys. Res.,* **102**, 3345-3355.

Kawamura, T., K. Shirasawa, N. Ishikawa, A. Lindfors, K. Rasmus, M.A. Granskog, J. Ehn, M. Leppäranta, T. Martma and R. Vaikmäe, 2001. Time-series observations of the structure and properties of brackish ice in the Gulf of Finland, *Ann. of Glaciol.,* **33**, 1-4.

Koh, G. and R. Jordan, 1995. Sub-surface melting in a seasonal snow cover, *J. Glaciol*., **41 (139)**, 474-482.

Kolkki, 1969. A review on the climate in Finland. *Ilmat. Lait. Tied.,* **18**. (in Finnish)

Launiainen, J. (Editor), 1999. *BALTEX-BASIS Data Report 1998,* Geesthacht, Germany. International BALTEX secretariat. (Publication **14**).

Launiainen, J. and B. Cheng, 1998. Modelling of ice thermodynamics in natural water bodies, *Cold Reg. Sci. Technol.,* **27 (3)**, 153-178.

Leppäranta, M. and A. Seinä, 1982. Statistics of fast ice thickness along the Finnish coast, *Finnish Mar. Res.,* **249**, 62-71.

Leppäranta, M, 1983. A growth model for black ice, snow ice and snow thickness in subarctic basins, *Nordic Hydrol.*, **14**, 59-70.

Lundin, M., M. Moberg, B. Håkansson and M. Granskog, 1998. Ground, air and satellite data obtained during BASIS field experiment by the Swedish Meteorological and Hydrological Institute. In: Launiainen, J. (ed.), BALTEX-BASIS Data Report 1998. International BALTEX secretariat. Publication **14**, 14-25. Geesthacht, Germany

Lundin, M. and A. Omstedt, 2001. Modelling of snow influence on land fast ice thickness. In: Lundin, M., SAR Remote Sensing of Snow Covered Sea Ice in Brackish Water-Investigation from the Baltic Sea. Licentiate thesis, Department of Radio and Space Science, School of Electrical and Computer Engineering, Chalmers University of Technology, Göteborg, Sweden.

Jacobs, J.D, 1978. Radiation climate of Broughton Island. In: Barry, R.G., and J.D. Jacobs, (eds), Energy budget studies in relation to fast-ice breakup processes in the Davis Strait. *Occas, Pap*. **26**, 105-120. Inst. of Arctic and Alp. Res., Univ. of Colorado, Boulder.

Liston, G.E., J.G. Winther, O. Bruland, H. Elvehoy and K. Sand, 1999. Below-surface ice melt on the coastal Antarctic ice sheet, *J. Glaciol*., **45 (150)**, 273-285.

Maykut, G.A. and N. Untersteiner, 1971. Some results from a time dependent thermodynamic model of sea ice, *J. Geophys. Res.,* **76 (6)**, 1550-1575.

Parkinson, C.L. and W.M. Washington, 1979. A large-scale numerical model of sea ice, *J. Geophys. Res.,* **84 (C1),** 311-337.

Paterson, W.S.B., 1983. *The Physics of Glaciers* (Second Edition), Pergamon Press. 379 pp.

Perovich, D.K., 1996. The optical properties of sea ice, *CRREL Rep.* **96-1**.

Pfeffer, W.T., T.H. Illangasekare and M.F. Meier, 1990. Analysis and modelling of melt-water refreezing in dry snow, *J Glaciol.,* **36 (123)** 238-246.

Pfeffer, W.T., M.F. Meier and T.H. Illangasekare, 1991. Retention of Greenland runoff by refreezing: implications for projected future sea level change, *J. Geophys. Res.,* **96 (C12)**, 22,117-22,124.

Pfeffer, W.T. and N.F. Humphrey, 1996. Determination of timing and location of water movement and ice-layer formation by temperature measurements in sub-freezing snow, *J. Glaciol*., **42 (141)**, 292-304.

Pfeffer, W.T. and N.F. Humphrey, 1998. Formation of ice layers by infiltration and refreezing of meltwater. *Ann. of Glaciol.,* **26**, 83-91.

Sahlberg, J., 1988. Modelling the thermal regime of a lake during the winter season, *Cold Reg. Sci. Technol*., **15 (2)**, 151-159.

Saloranta, T., 2000. Modelling the evolution of snow, snow ice and ice in the Baltic Sea, *Tellus* **52A**, 93-108.

Schlatter, T.W., 1972. The local surface energy balance and subsurface temperature regimes in Antarctica, *J. Appl. Meteorol.*, **11 (10)**, 1048-1062.

Semtner, A.J., 1976. A model for the thermodynamic growth of sea ice in numerical investigation of climate, *J. Phys. Oceanogr.*, **6**, 379-389.

Shine, K.P., 1984. Parameterization of short wave flux over high albedo surfaces as a function of cloud thickness and surface albedo, *Q. J. R. Meteorol. Soc.*, **110**, 747-764.

Shirasawa, K., K. Kobinata, and T. Kawamura, 2001. Eddy flux measurements below ice and ocean boundary layer studies. In: Launiainen, J. and T. Vihma, (eds), BALTEX-BASIS Final Report 2001. *International BALTEX Secretariat. Publication* **19**, 170-178. Geesthacht, Germany.

Sturm, M., J. Holmgren, M. König and K. Morris, 1997. The thermal conductivity of seasonal snow, *J. Glacoil.,* **43 (143)**, 26-40.

Untersteiner, N., 1961. On the mass and heat budget of Arctic sea ice, *Arch. Meteorol. Geophys. Bioklimatol*., **A 12**, 151-182.

Vihma, T., J. Uotila, B. Cheng, T. Purokoski, P. Kosloff, J. Launiainen and C. Schrum, 1998. Marine meteorological sea ice and oceanographic observation by the Finnish Institute of Marine Research. In: Launiainen, J. (ed.), BALTEX-BASIS Data Report 1998. *International BALTEX secretariat. Publication* **14**, 14-25. Geesthacht, Germany.